

Numerical Assessment of the Maximum Operating Pressure for SAGD Projects by Considering the Intrinsic Shale Anisotropy

^aEhsan Rahmati, ^bAlireza Nouri, ^cVahidoddin Fattahpour, ^dJapan Trivedi

^aUniversity of Alberta, Edmonton, Canada (Email: rahmatisina@gmail.com)

^bUniversity of Alberta, Edmonton, Canada (Email: anouri@ualberta.ca)

^c**Corresponding Author**, University of Alberta, Edmonton, Alberta, Canada (Email: fattahpo@ualberta.ca)

Room 3-133, NREF Markin/CNRL Department of Civil & Environmental Engineering, University of Alberta, Edmonton, Alberta, T6G 2W2, Canada

Phone: (780) 492-4117

Cell: (780) 802-7427

^dUniversity of Alberta, Edmonton, Canada (Email: jtrivedi@ualberta.ca)

Abstract

This paper investigates the effect of anisotropic behavior of caprock shales on the caprock failure pressure in SAGD projects. Shales and mudstones exhibit strong anisotropy at the micro and macro scales. However, the anisotropic behavior has been neglected in the existing published works on this subject. This paper focuses on the effect of the intrinsic anisotropy of shales on caprock integrity. The Maximum Operating Pressure (MOP) is calculated from the failure pressure using an appropriate safety factor.

In this paper, a coupled hydro-thermo-mechanical model was developed for the assessment of caprock integrity in thermal operations. A transversely isotropic constitutive model in the elastic range was combined with an anisotropic failure criterion to capture the intrinsic anisotropy of the cap shale. The coupled tool was validated against field data (mainly the surface heave) and employed in a study to determine the effect of shale anisotropic behavior on the pressure associated with caprock breach.

Results display the effect of shale anisotropy on caprock response in terms of deformations, stresses and failure pressure. The assumption of isotropic shale behavior in caprock integrity assessment for a case study resulted in the overestimation of the failure pressure by about 7%.

Existing numerical models for evaluating the integrity of caprocks during thermal operations employ isotropic constitutive laws. These models are believed to be deficient in capturing strongly anisotropic response of shales and mudstones. The research described in this paper incorporated elasto-plastic shale anisotropy in the caprock failure analysis model for the first time. This study demonstrates the importance of capturing shale anisotropy in the accurate prediction of caprock breach pressure in SAGD projects.

Keywords: SAGD, Maximum Operation Pressure (MOP), Shale, Caprock integrity, Intrinsic anisotropy, Coupled numerical modeling

1. Introduction

Steam injection into the reservoir increases the reservoir pressure and temperature during the Steam Assisted Gravity Drainage (SAGD) operation. The increase in pressure and temperature results in the expansion of the reservoir rock in the steam chamber and the alteration of stresses in the chamber and surrounding strata. As a result, localized shear and/or tensile failure can develop in the caprock, which may compromise the caprock integrity. Loss of caprock integrity could result in irrecoverable consequences for the reservoir and environment.

Shales comprise the majority of sedimentary rocks that are drilled to reach the hydrocarbon reservoir. As a result, shale studies have been at the forefront of research in the petroleum industry (Tutuncu, 2010). Experimental evidence indicates that most sedimentary rocks, particularly shales and mudstones, behave anisotropically (Karakul et al., 2010; Kwasniewski, 1993; Ramamurthy, 1993; Horino and Ellickson, 1970; McLamore and Gray, 1967; Hoek, 1964; Donath, 1964). Shales exhibit strong inherent anisotropy due to the existence of bedding planes and the platelet shape of shale grains. This anisotropy manifests itself in directional dependency of deformation and strength properties (Duveau et al., 2001). Despite several efforts for the study of caprock integrity in SAGD projects (Rahmati et al., 2013; Khan et al., 2011; Chalaturnyk, 2011; Collins, 2007; McLellan and Gillen, 2000; Smith, 1997), the anisotropic elasto-plastic behavior of the shale/mudstone strata has not been accounted for in caprock integrity investigations.

In this study, a coupled hydro-thermo-mechanical model was developed to assess caprock integrity in thermal recovery operations. A transversely isotropic constitutive model in the elastic range was combined with an anisotropic Mohr-Coulomb (MC) strength criterion based on variable cohesion and friction angle theory proposed by McLamore and Gray (1967) to capture the intrinsic anisotropic characteristics of caprock shale. The proposed model simulated the variable state of stress and deformation using a geomechanical module sequentially coupled with a reservoir simulator. The failure pressure for steam injectors was calculated and compared for the corresponding isotropic and anisotropic cases.

2. Theoretical Background

Caprock usually consists of shale layers that contain different constituent minerals. The two primary types are clay minerals and framework silicates that are usually quartzic (Pettijohn, 1957). Elastic properties of shale are strongly anisotropic (Sone, 2012). Typical shales have quartz content in the range of 30-40 percent and clay content that frequently exceeds 50 percent (Hemsing, 2007). Preferred orientation of clay minerals is one of the sources of anisotropy in shales. Further, stratification of shale formations leads to transversely isotropic symmetry (Hemsing, 2007).

In an elastic medium with transversely isotropic symmetry and plane strain condition, stress and strain are related by the Hooke's law as follows (Puzrin, 2012):

$$\begin{Bmatrix} \varepsilon_{xx}^e \\ \varepsilon_{yy}^e \\ \varepsilon_{zz}^e \\ \varepsilon_{xy}^e \end{Bmatrix} = \begin{bmatrix} 1/E_h & -\nu_{vh}/E_v & -\nu_{hh}/E_h & 0 \\ -\nu_{hv}/E_h & 1/E_v & -\nu_{hv}/E_h & 0 \\ -\nu_{hh}/E_h & -\nu_{vh}/E_v & 1/E_h & 0 \\ 0 & 0 & 0 & 1/2G_{hv} \end{bmatrix} \begin{Bmatrix} \sigma_{xx} \\ \sigma_{yy} \\ \sigma_{zz} \\ \sigma_{xy} \end{Bmatrix} \quad (1)$$

where σ is the second-order stress tensor; ε is the second-order strain tensor; E_h and E_v are the Young moduli in the horizontal and vertical directions, respectively; G_{hv} is the cross-shear modulus between a plane of isotropy and the perpendicular plane; ν_{ab} is the Poisson's ratio, where "a" indicates the stress direction (vertical v or horizontal h), and "b" indicates the direction of the strain component (also vertical v or horizontal h) caused by this stress. Above formulation has five independent constants: $E_h, E_v, \nu_{hh}, \nu_{vh}, \nu_{hv}$. Components of the stress tensor in 3D are shown in Figure 1.

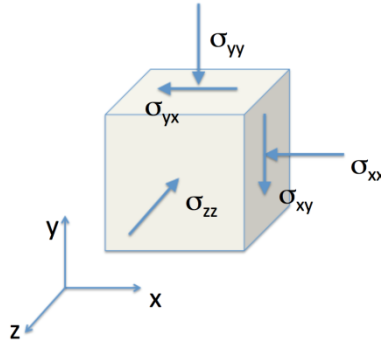


Figure 1. Components of stress tensor for plane strain condition

Lekhnitskii (1981) suggested the following formula based on experimental data to calculate cross-shear modulus.

$$G_{hv} = \frac{E_v E_h}{E_h(1 + 2\nu_{hv}) + E_v} \quad (2)$$

Several researchers (Niandou et al., 1997; McLamore and Gray, 1967; Donath, 1964) showed that the strength parameters and deformation characteristics of shale rocks are highly dependent on the orientation of anisotropy with respect to the principal stress directions.

McLamore and Gray (1967) proposed a theory with variable cohesion and friction angle for sedimentary rocks, especially shales. Based on triaxial test results, they proposed the following formulae for the angular variation of cohesion and friction angle:

$$c(\theta) = A_{1,2} - B_{1,2} \cos \left(2(\theta_{min,c} - \theta) \right)^n \quad (3)$$

$$\varphi(\theta) = \arctan \left(C_{1,2} - D_{1,2} \cos \left(2(\theta_{min,\varphi} - \theta) \right)^m \right) \quad (4)$$

where θ is the angle between the maximum principal stress and the bedding plane direction; $c(\theta)$ and $\varphi(\theta)$ are cohesion and friction angle, respectively; $\theta_{min,c}$ and $\theta_{min,\varphi}$ are the value of θ corresponding to the minimum cohesion and friction angle, respectively; A_1, B_1 and C_1, D_1 are constants that describe the variance over the range of $0^\circ \leq \theta \leq \theta_{min,c}$ and $0^\circ \leq \theta \leq \theta_{min,\varphi}$, respectively; A_2, B_2 and C_2, D_2 are constants that describe the variance over the range of $\theta_{min,c} < \theta \leq 90^\circ$ and $\theta_{min,\varphi} < \theta \leq 90^\circ$, respectively; n and m are "anisotropy type" factors and have the value of 5 or 6 or greater for the linear type of anisotropy associated with bedding planes (McLamore and Gray, 1967).

We used the variable cohesive strength and friction angle theory (McLamore and Gray, 1967) in conjunction with the Mohr-Coulomb criterion for describing the cap shale behaviour. A tension cut-off was adopted as the tensile yield criterion. Non-associated and associated flow rules were adopted in the shear and tensile constitutive models, respectively. The models were embedded in FLAC software for the analysis of caprock integrity.

3. Numerical Model

Conventional SAGD simulations consider fluid and heat flow in the reservoir, but often neglect geomechanical processes. The main geomechanical processes include shearing, dilation, and possible tensile fracturing (Uwiera-Gartner et al., 2011). These processes can change the material properties such as porosity and permeability, thus the reservoir fluid and heat flow (Azad and Chalaturnyk, 2011). A coupled hydro-thermo-mechanical model is required to capture various important phenomena in and around the SAGD reservoir.

Different aspects of the numerical model including the modeling scheme, case study, geometry, boundary conditions, and input data will be discussed in this section.

3.1. Hydro-thermo-mechanical Coupled Model

We utilized and linked two commercial finite difference software packages (FLAC, geomechanical software package developed by ITASCA (Itasca Consulting Group, 2011) and STARS, flow simulator developed by CMG (CMG, 2013) to perform the simulations. A MATLAB code was used as an interface to run the modules and also update the shared parameters (see Figure 2). The simulations within each time step were iterated between FLAC and STARS. STARS calculated the pressures and temperatures that were transferred to FLAC where stresses and deformations were calculated. The deformations were then used to update the porosities and permeabilities in the entire reservoir space. The porosities and permeabilities were then transferred to STARS for the next flow-temperature iteration. The iterations within each time step continued till convergence was achieved in each time step. Convergence tolerance of 5% was considered for pressure, temperature, porosity, and permeability at each time step.

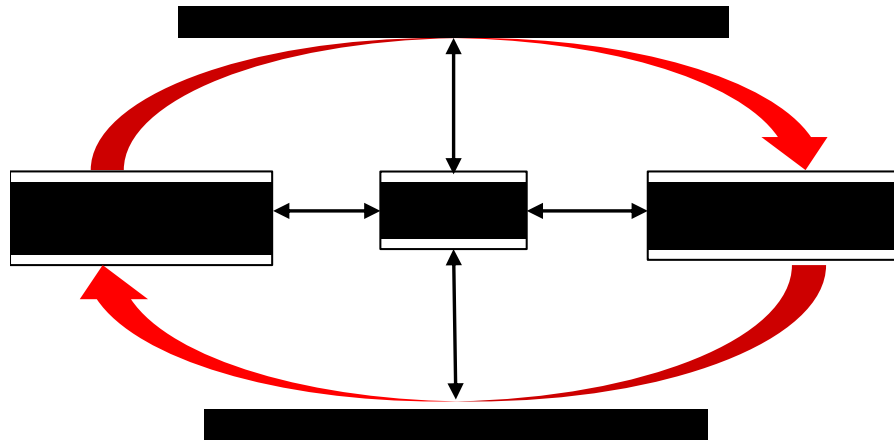


Figure 2. Sequential coupling scheme (after Rahmati et al., 2014)

Equations proposed by Touhidi-Baghini (1998) were used to relate permeability and porosity to the sand volume change. The equations are as follows:

$$\ln\left(\frac{K}{K_0}\right) = \frac{\beta}{\phi_0} \varepsilon_V \quad (5)$$

$$\phi = \frac{\phi_0 + \varepsilon_V}{1 + \varepsilon_V} \quad (6)$$

where K is permeability, ϕ is porosity, and the subscript '0' indicates initial permeability and porosity. In this study, β was assumed to be 2 and 5 for horizontal and vertical permeability, respectively (Azad and Chalaturnyk, 2011).

3.2. Case Study

We used public data related to Pad C of McKay River oil sands project (Suncor Energy Inc., 2009) located northwest of Fort McMurray, Alberta, Canada as the case study. We had to assume some input parameters since not all variables were publicly available. As such, this work should not be considered as caprock investigation for this particular project. Rather, it should be seen as an effort to improve the understanding on the impact of anisotropy on failure pressure. Steam circulation for this project commenced in September 2002 in the original 25 well pairs (Petro-Canada Corp., 2005a). Surface heave data for this project are available between 2002 and 2008 (Suncor Energy Inc., 2009).

Log data for Pad C indicate the thicknesses of different formations from top to bottom: Quaternary Deposits (40 m), Clearwater shale (40 m), Wabiskaw member (20 m), McMurray formation (30 m), and Devonian limestone (underburden rock) (Suncor Energy Inc., 2009). Clearwater formation, which is considered as the main caprock (Southern Pacific Resource Corp., 2012), consists of different layers of mudstone, shale, siltstone and sandstone. For simplicity, Clearwater formation shale was assumed as homogenous anisotropic shale in terms of hydraulic and mechanical properties. Similarly, Wabiskaw member, which consists, from top to bottom, of (1) Wabiskaw A shale, (2) gas-saturated Wabiskaw C sand, and (3) the lower-most Wabiskaw D mudstone (ERCB, 2010), was considered as a homogenous layer with mechanical properties equivalent to Wabiskaw A shale.

Figure 3 shows the principal stress directions in relation to the wellbore trajectory in the area of interest. Pad-C wells were drilled parallel to the maximum horizontal stress. Principal in-situ stresses have been interpreted based on well log data, minifrac test data, and tectonic strain hysteresis. Average stress gradients as well as pore pressure profile for each stratigraphic zone in this area are shown in Figure 4 (Walters et al., 2012). In this figure, the solid lines are based on the work of Walters et al. (2012), but the dashed lines are based on educated assumptions regarding the recorded trends for in situ stresses in Western Canada Basin (Bell and Babcock, 1986).

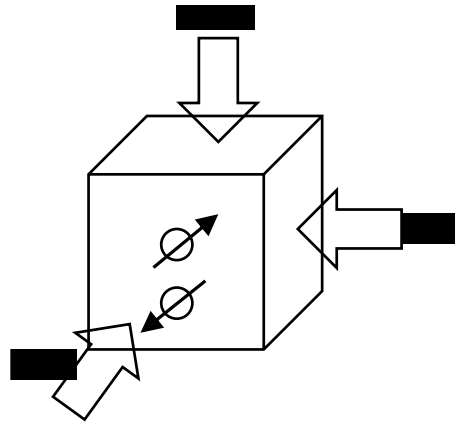


Figure 3. Principal stress directions

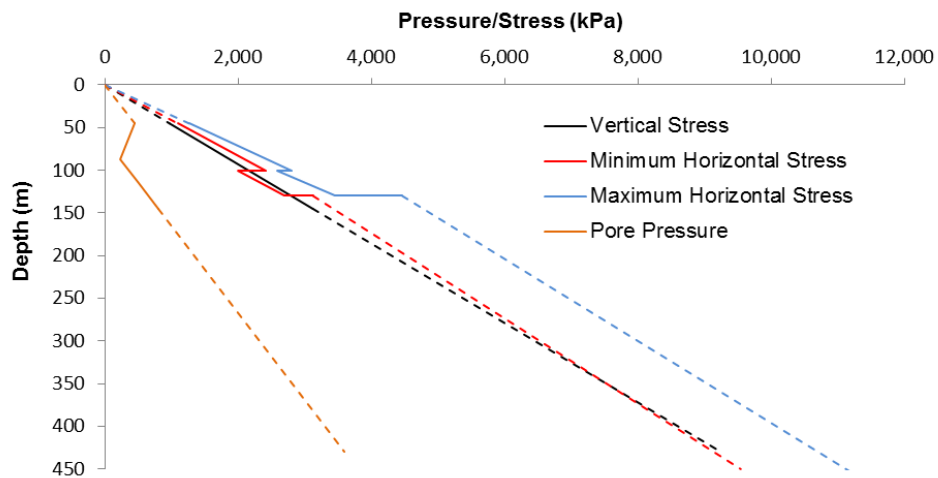


Figure 4. In-situ stress and pore pressure profiles

3.3. Geometry, Boundary Conditions, and Operational Conditions

A cross-section of Pad C was simulated by assuming 2-D plane strain condition (no deformation along the horizontal wells). This approach is deemed applicable for this problem because (1) the length of wellbores is large in comparison with the distance between the wells; (2) thermocouple measurements show uniform distribution of temperature along the producers (Suncor Energy, 2013). The latter indicates relatively uniform steam injection and production along the wells.

There are 6 well pairs called C1 to C6 in Pad C, which were reduced to only three in the model assuming symmetric geometry and operation (Figure 5). The model length and depth were chosen large enough to minimize boundary effects on the results.

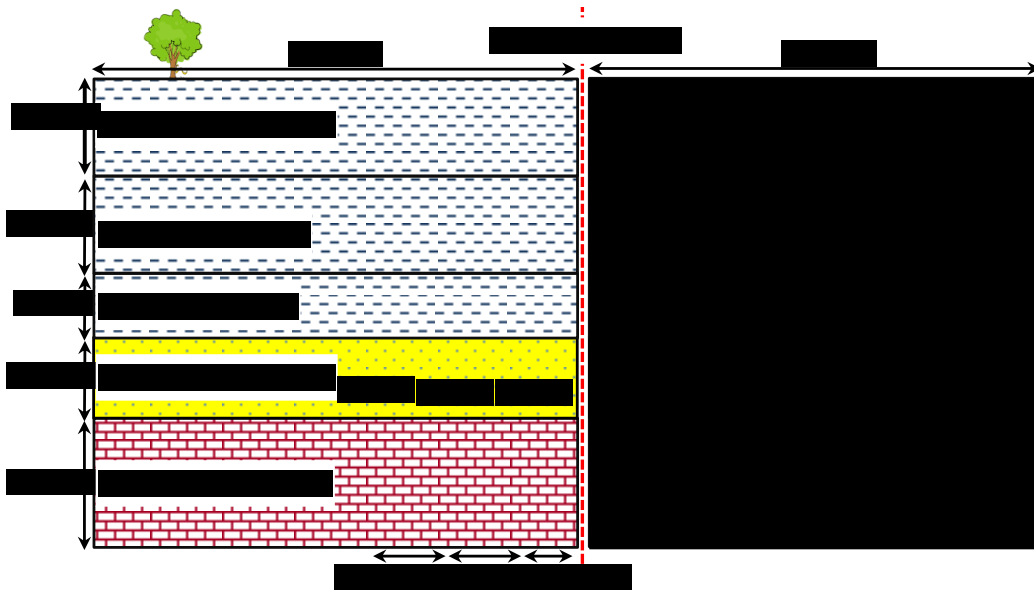


Figure 5. Model geometry

Side boundaries of the model were fixed in the horizontal direction and the bottom boundary was fixed in the vertical and horizontal directions. Due to the symmetry assumption, no heat/fluid flow was considered at the right boundary of the model. Pressure and temperature at the left boundary of the model were considered to be unaffected by the pad operation. Preheating period of 90 days was simulated and the pad production was simulated using the injection and production data from September 2002 to January 2008.

Figure 6 illustrates numerical mesh design for the geomechanical analysis. Different element sizes were used in the geomechanical model to reduce the computation time of the coupled model. Continuous $2\text{ m} \times 1\text{ m}$ element size was used in the fluid flow simulator (see Figure 7). The total number of elements in the geomechanical and fluid flow models were 26,500 and 92,000, respectively. Coupling parameters (pressure, temperature, porosity, and permeability) were mapped from one module to another by using the cubic spline data interpolation method (Michiel, 2001).

In this paper, we simulated five years of field operations. Steam quality, temperature, and pressure were reported to be 95%, 200 °C and 1,650 kPa, respectively (Suncor Energy, 2009). Steam circulation for this project commenced in September 2002 in the original 25 well pairs (Petro-Canada Corp., 2005a). Actual injection-production data were used for the first 5 years of the operation. Injection-production rates are not shown on this paper due to the data confidentiality.

3.4. Input data

The material and fluid properties have been chosen from laboratory tests, geophysical logs, and field testing in published papers and technical reports. For those parameters that were not available, data from similar SAGD projects were assumed. Major references used for the input data were: Chalaturnyk (1996), Thomas and Sands (2010), Uwiera-Gartner et al. (2011), and Southern Pacific Resource Corp. (2012). Hydraulic, thermal, and mechanical input data are summarized in Table 1, Table 2, and Table 3, respectively.

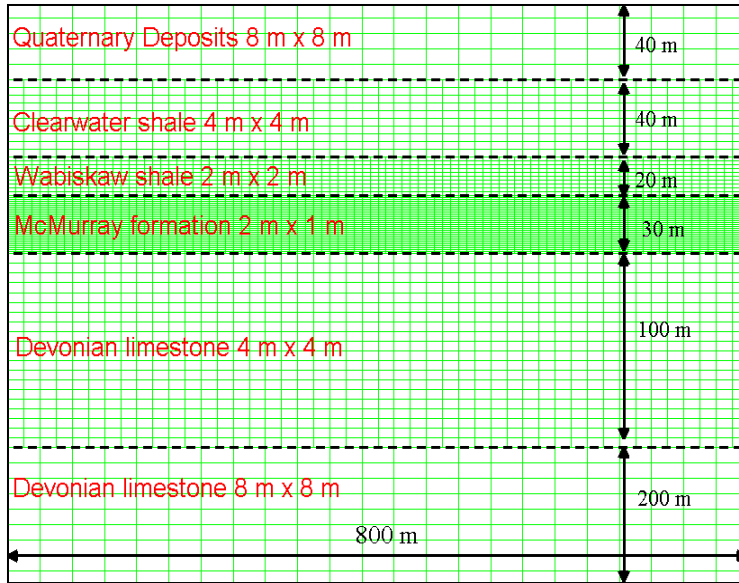


Figure 6. Geomechanical grid-block size for each layer

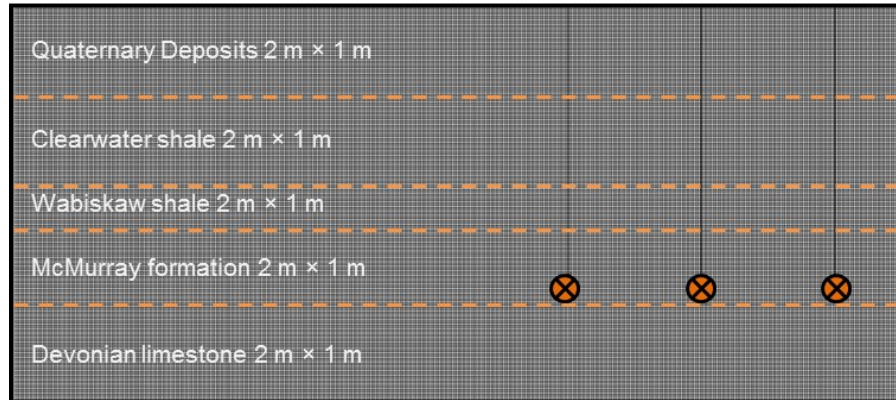


Figure 7. Fluid flow grid-block size for each layer

Table 1. Permeability in different layers

Zone	Horizontal permeability (mD)	Vertical permeability (mD)	Reference
Clearwater shale	0.001	0.001	AER (2014)
Wabiskaw A shale	0.001	0.001	ERCB (2010)
Wabiskaw C sand	2,000	2,000	ERCB (2010)
Wabiskaw D mudstone	0.001	0.001	ERCB (2010)
McMurray formation	6,400	3,400	Petro-Canada Corp. (2005b)
Devonian limestone	¹ 115	² 0.001	¹ Uwiera-Gartner (2011) ² Thomas and Sands, (2010)

Table 2. Thermal properties of the reservoir layer

Parameter	Value	Reference
Rock Expansion Coefficient ($1/^\circ\text{C}$)	3.84e-5	Chalaturnyk (1996)
Rock Thermal Conductivity ($\text{W}/\text{m}\cdot^\circ\text{K}$)	1.736	Chalaturnyk (1996)
Rock Heat Capacity ($\text{kJ}/\text{kg}\cdot^\circ\text{K}$)	1865	Chalaturnyk (1996)

Table 3. Isotropic geomechanical properties of model for caprock and underburden layers

Zone	Formation	Parameter	Value	Reference
<i>Overburden</i>	Quaternary Deposits	Young's modulus (MPa)	25	Uwiera-Gartner et al. (2011)
		Poisson's ratio	0.45	Uwiera-Gartner et al. (2011)
		Cohesion (kPa)	200	Thomas and Sands (2010)
		Friction Angle ($^\circ$)	25	Thomas and Sands (2010)
	Clearwater shale	Young's modulus (MPa)	$^1E=76.67\sigma_3+23.33$	Kosar (1989)
		Poisson's ratio	0.13	Thomas and Sands (2010)
		Cohesion (kPa)	200	Thomas and Sands (2010)
		Friction angle ($^\circ$)	25	Thomas and Sands (2010)
	Wabiskaw shale	Young's modulus (MPa)	250	Kosar (1989)
		Poisson's ratio	0.15	Kosar (1989)
		Cohesion (kPa)	1,085	Khan et al. (2011)
		Friction angle ($^\circ$)	20	Khan et al. (2011)
<i>Under-burden</i>	Devonian limestone	Young's modulus (MPa)	1,500	Chalaturnyk (1996)
		Poisson's ratio	0.3	Thomas and Sands (2010)
		Cohesion (kPa)	200	Thomas and Sands (2010)
		Friction angle ($^\circ$)	40	Thomas and Sands (2010)

¹based on Kosar (1989) triaxial tests. E is Young's modulus and σ_3 is effective confining pressure.

Note the mechanical properties in Table 3 have been obtained by laboratory testing on vertical core samples (i.e., sample axis being perpendicular to sedimentary layers). For Quaternary deposits and Devonian limestone, the same properties were assumed to be valid for all other directions (this paper focuses on the investigation of the effect of anisotropy of caprock layers, therefore,

anisotropy in other layers is neglected). For Clearwater and Wabiskaw shale, the numbers were assumed to be applied only for the vertical direction and the properties in all other directions were determined based on the discussions in this section.

Sone (2012) proposed the following empirical formula to calculate the ratio of horizontal to vertical Young's modulus for shales with caly content in the range of 5% and 65%:

$$\frac{E_h}{E_v} = 3.1 \exp(-0.0195 E_v (GPa)) \quad (7)$$

where E_h and E_v are horizontal and vertical Young's moduli, respectively.

Equation above was used to calculate the horizontal Young's modulus at different confining pressures for Clearwater shale and Wabiskaw shale. Table 4 lists the Poisson's ratios for Clearwater and Wabiskaw shale. The Poisson's ratio (ν_{hv}) was calculated based on the following relationship (Eq. 8) (Puzrin, 2012). The Poisson's ratio (ν_{hh}) was observed to be close to (ν_{vh}) according to experimental data provided by Sone (2012). In this paper, those were assumed to be equal.

$$\frac{\nu_{hv}}{\nu_{vh}} = \frac{E_h}{E_v} \quad (8)$$

Table 4. Transversely isotropic properties of anisotropic layers

Formation	Property	Value
Clearwater shale	Poisson's ratio (ν_{hv})	0.40
	Poisson's ratio (ν_{vh}, ν_{hh})	0.13
Wabiskaw shale	Poisson's ratio (ν_{hv})	0.45
	Poisson's ratio (ν_{vh}, ν_{hh})	0.15

Correlations by McLamore and Gray (1967) were adopted to calculate the cohesion and friction angle in different directions for Clearwater/Wabiskaw shales. The strength properties of anisotropic layers are presented in Figure 8. In this figure, θ is the angle between the maximum principal stress and the horizontal direction. In Figure 8, the strength properties for the vertical direction ($\theta=90^\circ$) were adopted from the Table 3. The calibration parameters for the cohesion and friction angle in Eqs. 3 and 4 for the Clearwater and Wabiskaw shales were assumed to be the same as those of Green River shale (McLamore and Gray, 1967) (Table 5).

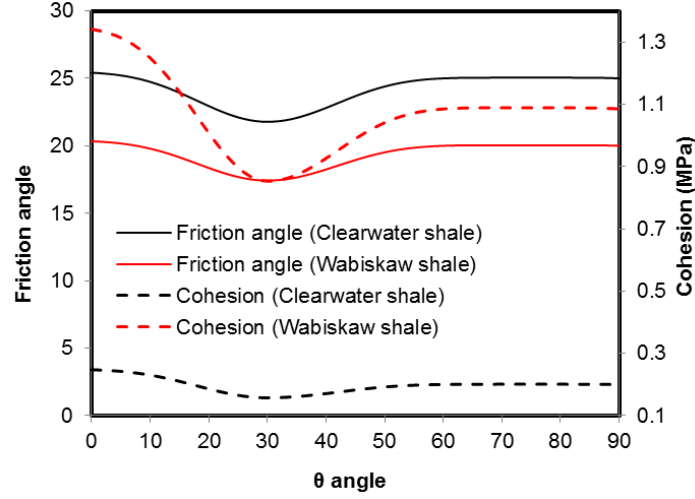


Figure 8. Friction angle and cohesion in different directions for anisotropic layers

Table 5. Calibration parameters for anisotropic layers

Parameter	Clearwater shale	Wabiskaw shale	Parameter	Clearwater shale	Wabiskaw shale
A1	2.5e5	1.34e6	C2	0.466	0.349
A2	2e5	1.085e6	D1	0.06	0.051
B1	9e4	4.88e5	D2	0.056	0.045
B2	4.3e4	2.32e5	m	6	6
C1	0.475	0.355	n	6	6

Isotropic stress-strain behavior was assumed for McMurray formation. Li and Chalaturnyk (2005) showed that following relationship is appropriate to represent the modulus of elasticity variation behavior of oil sands in Athabasca oil sands, Alberta.

$$E = 950 P_a (\sigma_3/P_a)^{0.5} \quad (8)$$

where, E is Young's modulus; σ_3 is minimum principal effective stress, and P_a is atmospheric pressure.

A bilinear Mohr-Coulomb yield function was implemented for the oil sands, which was also used by Nouri et al. (2009). Li and Chalaturnyk (2005) showed that the friction and dilation angle of oil sands are dependent on minimum effective principal stress. They proposed the following equations for the friction angle and dilation angle of oil sands:

$$\varphi = 55 - 14.93 \log(\sigma_3/P_a) \quad (9)$$

$$\psi = 25.8 - 12.05 \log(\sigma_3/P_a) \quad (10)$$

where, ϕ and ψ are friction and dilation angle, respectively.

Based on the relations proposed by Li and Chalaturnyk (2005), friction angle and dilation angle for Low Effective Confining Stress (LECS) and High Effective Confining Stress (HECS) are presented in Table 6.

Table 6 Mechanical properties of oil sands

Zone	LECS	HECS
Friction angle	47°	35.7°
Dilation angle	19°	10.2°
Cohesion (kPa)	0	610

4. Results and Discussion

The coupled hydro-thermo-mechanical model was used to investigate the caprock integrity and determine the failure pressure for the case study problem. Numerical simulation was performed for both anisotropic and isotropic models for 5 years of pad operation to evaluate the impact of the anisotropic behavior of caprock shale on the failure pressure.

Measured surface heave data (Suncor Energy Inc., 2009) were used to validate the model (Figure 9). As depicted in Figure 9, the displacements from the anisotropic model show a better agreement with the measured data than those of the isotropic model. It seems that all calculated displacements in Figure 9 are smaller than measured data. Reasons could be, for instance, the possible use of smaller coefficient of thermal expansion or higher Young's modulus than the actual values. It may also be associated with effect of the temperature on cohesion, friction and Young's modulus, which haven't been considered in the analysis. As mentioned before, the input data were obtained from published data not necessarily for this particular site. Therefore, we are not looking for a perfect match. However the similarity of the results to the measured data seems to be promising and acceptable for such a complicated problem.

The difference between the vertical displacements for the isotropic and anisotropic models could be explained noting different values for caprock horizontal stiffnesses. The Young's modulus in the horizontal direction for the anisotropic model is about three times larger than the same in the isotropic model. Therefore, the predicted horizontal displacement in the anisotropic model is smaller than isotropic model. Thus, for the same amount of reservoir expansion, the anisotropic model results in larger vertical displacement in the reservoir and consequently larger heave at the surface.

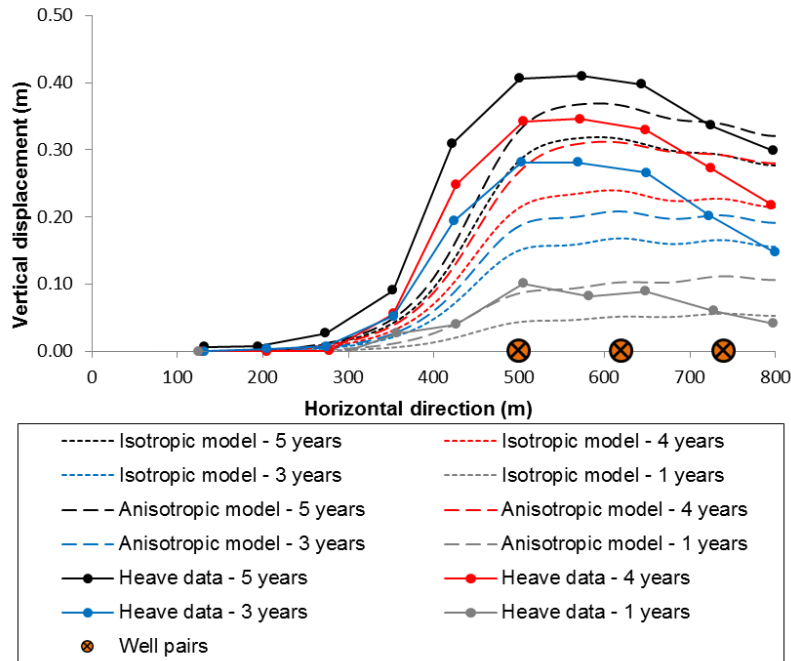


Figure 9. Comparison between the measured and calculated heave data

Pore pressure and temperature are among the main parameters that change during the SAGD operation. Steam injection causes the expansion of the steam chamber and evolution of the pore pressure and temperature during the operation (Figure 10). Results show the increase of reservoir pore pressure from the in situ level of 500 kPa to 1,650 kPa (injection pressure) during the growth of the steam chamber. Little pore pressure change is observed in the caprock during five years of operation, due to the low permeability of caprock shales, allowing minimal diffusion. The permeability of Wabiskaw C sand is large, defusing any pore pressure build-up due to the increase in temperature.

Unlike pore pressure, temperature has changed noticeably during the SAGD operation in both caprock shales and underburden limestone (see Figure 10). Temperature in Wabiskaw shale has increased up to 110 °C right above the steam chamber. The temperature change is negligible for the points closer to the interface of Wabiskaw and Clearwater shale. The temperature increase in the reservoir also affects the underburden rock. The temperature at the interface of Devonian limestone and the reservoir has increased by up to 120 °C. It is worth pointing out that the temperature change in the underburden limestone is limited to the close vicinity (approximately 20 m) of the reservoir.

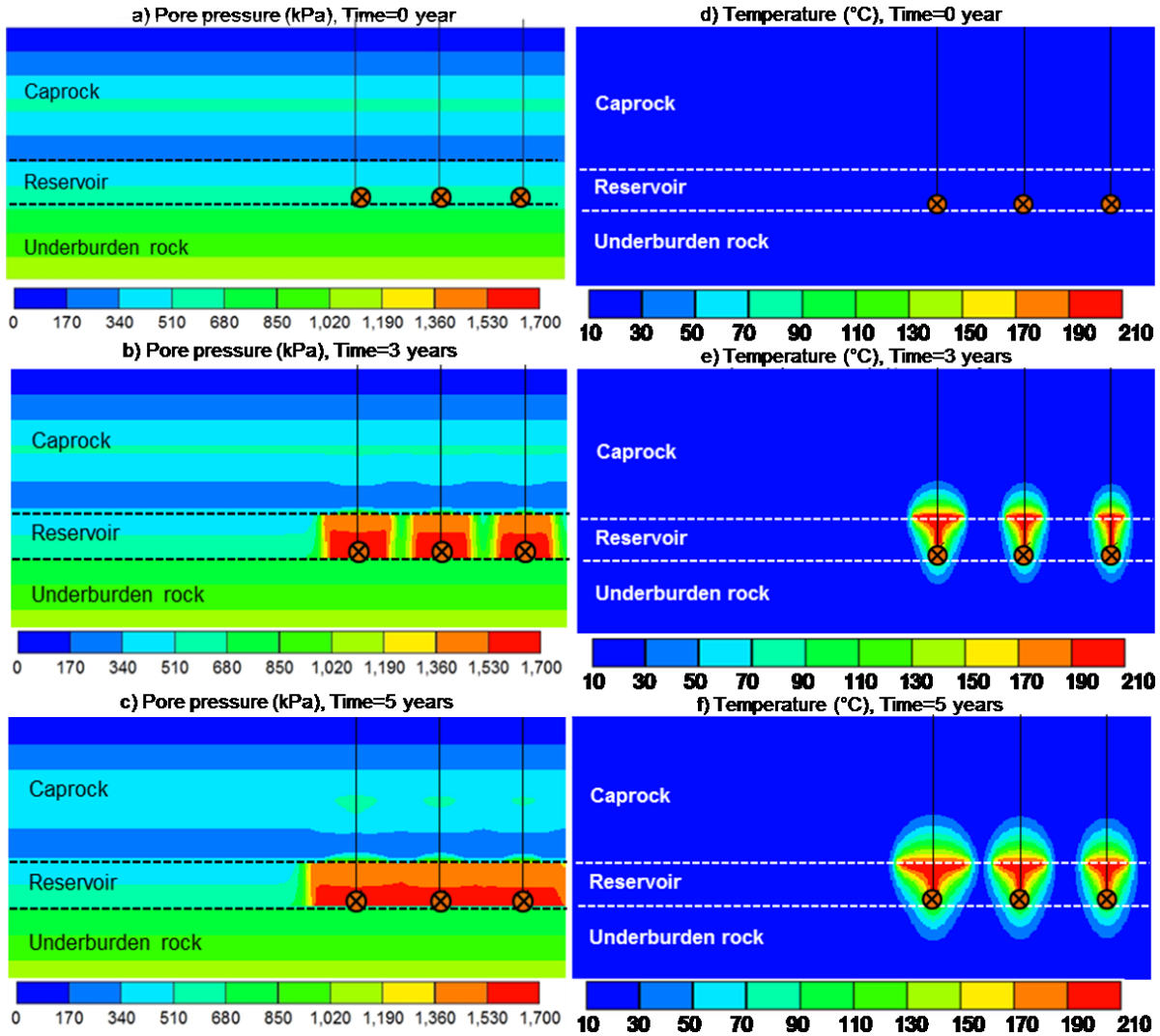


Figure 10. Pore pressure and temperature maps in the model: (a-c) pore pressure maps and (d-f) temperature maps

SAGD operation alters ground stresses in and around the reservoir due to reservoir expansion. Figure 11 depicts the total horizontal stress profile for different vertical sections at different distances of 250 m, 450 m and 500 m from the left boundary of the model. Horizontal stress profile for Section A is nearly unaltered from the initial state because of the relatively large distance from the SAGD wells. For Sections B and C, however, horizontal stresses are higher at the reservoir interval due to increased pore pressures and the thermal expansion of the reservoir sand. The total horizontal stresses in the overburden and underburden layers decrease from the original values to compensate for the increased horizontal stresses at the reservoir interval. Figure 11 shows that the horizontal stress profiles for the isotropic and anisotropic cases do not match and the maximum difference is as large as 29% with respect to the horizontal in-situ stress (Figure 11c-d). Both models predict similar horizontal stress trends for Quaternary deposits, the reservoir and underburden layers.

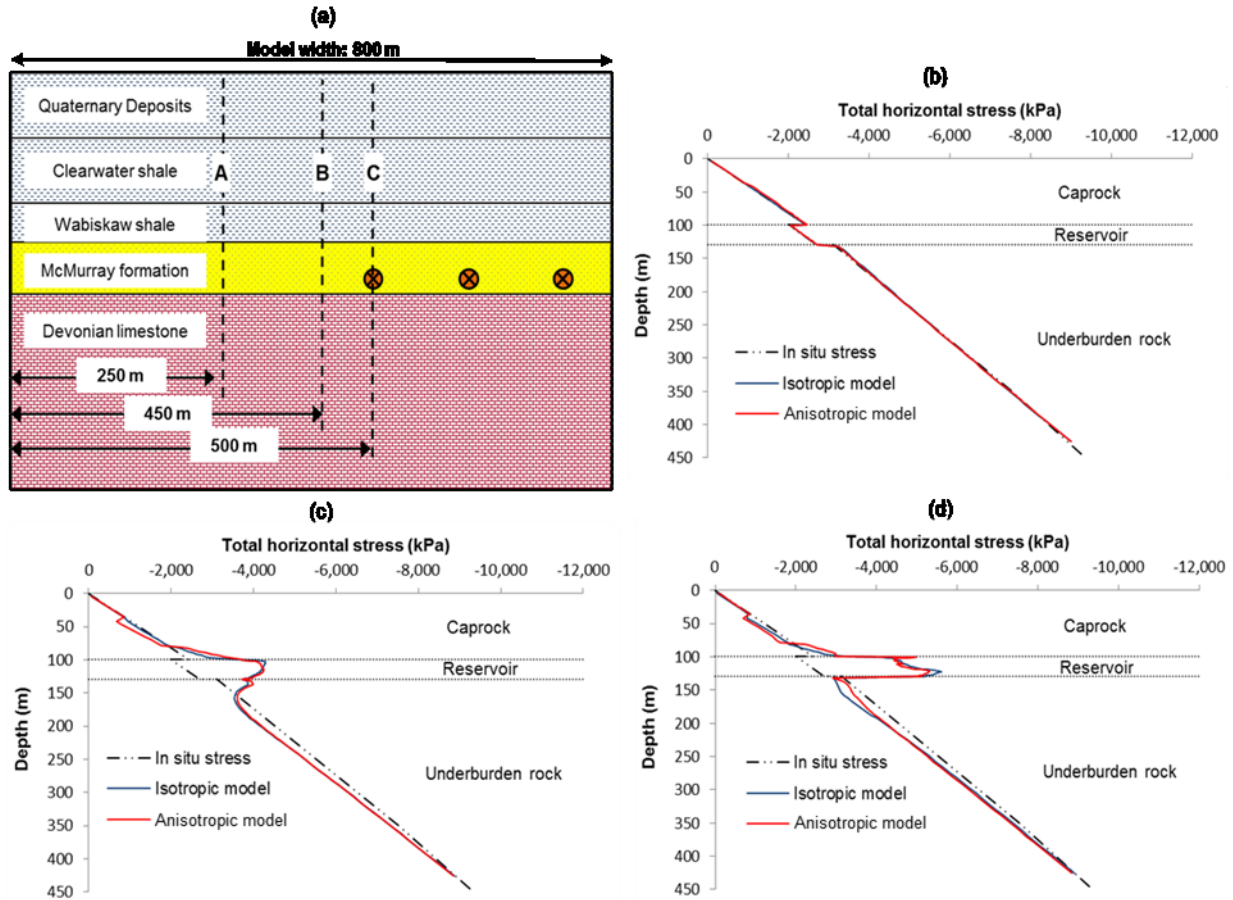


Figure 11. Total horizontal stress profile for vertical sections after 5 years of operation a) Vertical cross section locations, b) Total horizontal stress at cross section A, c) Total horizontal stress at cross section B, d) Total horizontal stress at cross section C

Figure 12 shows the total vertical stress profiles at different horizontal sections. Results indicate the vertical stresses in the cap shale are disturbed during the SAGD operations. Further, higher maximum and lower minimum for the vertical stress profiles result for the anisotropic model. Generally, the vertical stresses above the chamber increase while the same at the reservoir flanks decrease, a phenomenon, which is known as thermal jacking (Collins, 2006). This is because of the expansion of the reservoir sand in the chambers, which result in stronger compressive forces on the caprock in places directly above the wells. The stress drop at the reservoir flanks for the anisotropic model is found to be more significant than the same for the isotropic model. As expected far from the reservoir, stresses in both models converge to in situ stresses representing the fact that the model is large enough to avoid any boundary effects.

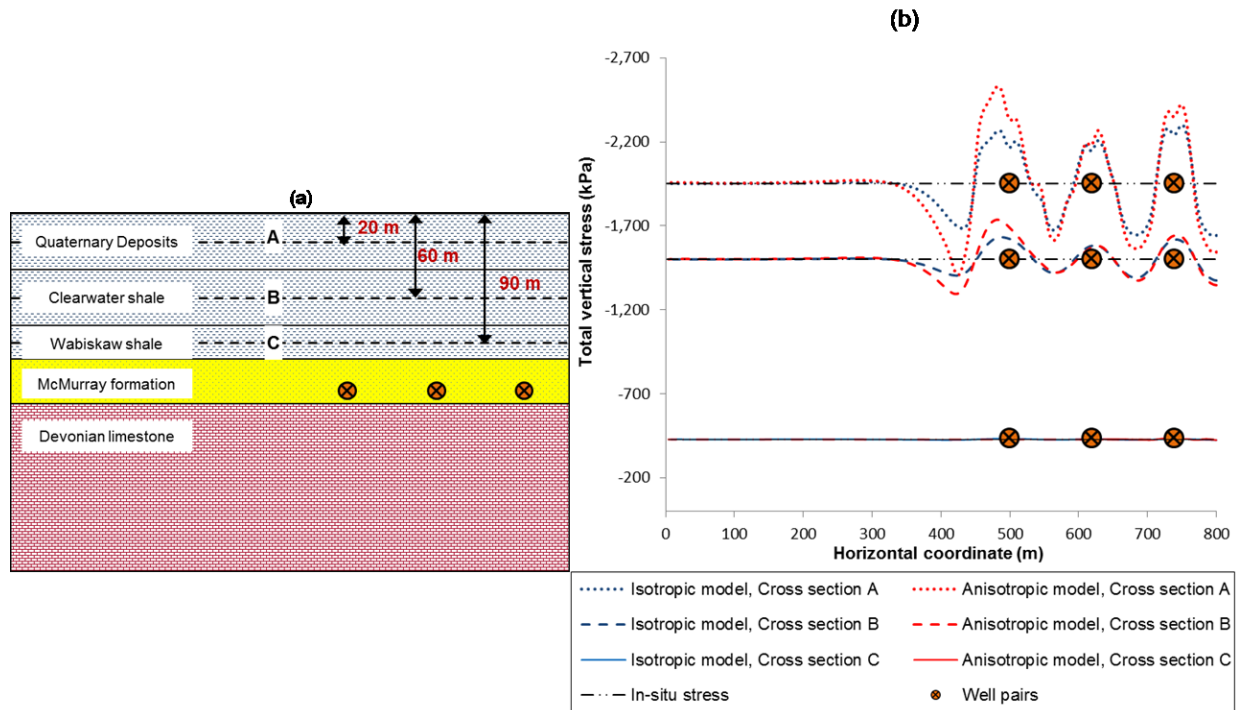


Figure 12. Total vertical stress at different horizontal sections, a) Horizontal cross section locations, b) total vertical stress in different cross sections after 5 years for both isotropic and anisotropic models

Figure 13 shows the stress contour map for the anisotropic model. For early stages of injection (3rd year) steam chambers are separate and thermal jacking is apparent as vertical stresses are higher than the in situ stresses above the well pairs and lower between the well pairs. Horizontal stresses in reservoir are significantly larger than the in situ stresses. Accordingly, horizontal stresses in the cap and base rocks are lower than in situ stress to satisfy the force equilibrium. As injection and production continues, steam chambers expand and eventually join together.

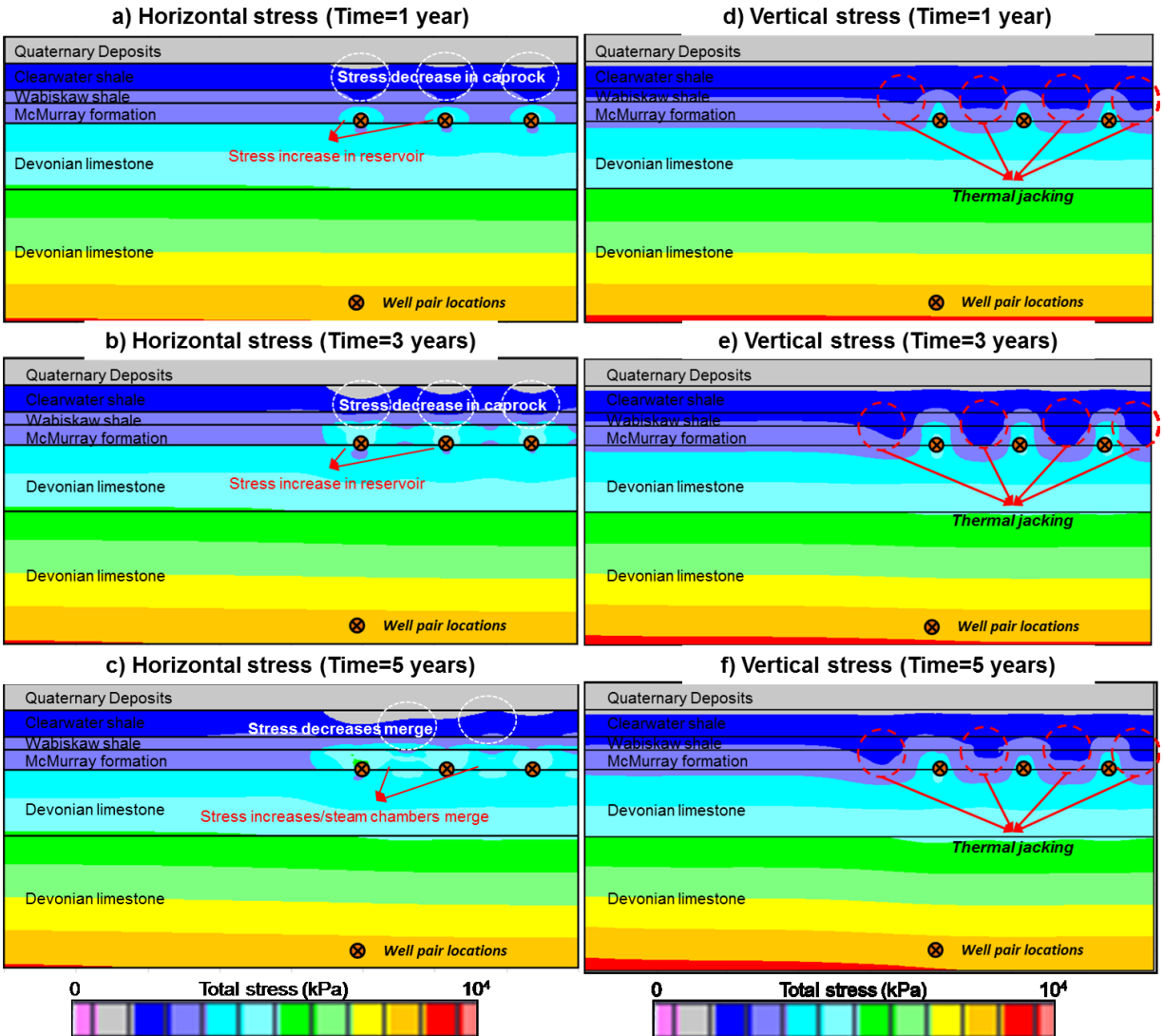


Figure 13. Total stress contour maps for anisotropic model during the production; a - c show horizontal stresses and d-f show vertical stresses

The main focus of this study was the determination of the injection pressure associated with the breach of caprock integrity (failure pressure). Simulation results indicate the injection pressures Suncor had used during the years 2002-2007 did not compromise the caprock. In an effort to determine the failure pressure, we increased the injection pressures in the simulations beyond the actual levels (see Figure 14). The injection pressures were increased in 10% steps (10% of the initial injection pressure at the end of five years of operation) and the pressure at each step was kept constant for six months. Injection pressures were increased until the caprock integrity was compromised, which meant the yielded zone had extended from the reservoir-caprock interface to the caprock-quaternary deposits interface. To obtain a more accurate prediction of failure pressure, after the occurrence of caprock breach, the numerical model for the last increment was repeated at 5% and 2.5% increments of the injection pressure, rendering failure pressure with higher accuracy than 40 kPa.

A sensitivity analysis was performed on the time intervals for the injection pressure ramp-up for the isotropic model (6, 12, and 24 months) to see if this duration influenced the failure pressure.

The failure pressure for different time intervals was found to be the same. It was observed that the initiation of caprock yield and the full expansion of the yielded zone in the caprock thickness occurred within the first 3 and 6 months of the interval, respectively.

According to Figure 14, the anisotropic model yielded at lower injection pressure than the isotropic model (2,392 kPa vs. 2,557 kPa). The failure pressure for the anisotropic and isotropic models were approximately 45% and 55% higher than the maximum operating injection pressure that had been exercised in the field, respectively. Figure 15 shows the growth of the yielded zone for the injection pressure of 2,392 kPa, which resulted in the breach of caprock integrity for the anisotropic model. According to Figure 15, yield initiated from the interface of Quaternary Deposits and Clearwater shale. This is due to lower effective stresses at shallower depths of the Clearwater shale, which is easily affected by reservoir expansion in a way that the stress state reaches the failure envelope.

Isotropic caprock would tolerate higher injection pressures (2,557 kPa) before the caprock breach. Figure 16 shows the growth of the yielded zone for the injection pressure of 2,557 kPa for the isotropic caprock.

The numerical model presented in this paper predicts the failure pressure and the yielded pattern in the caprock. The failure pressure can be converted to the Maximum Operating Pressure (MOP) if a reasonable safety factor is considered. The safety factor is meant to protect against uncertainties in the input data, and modeling limitations and assumptions. The safety factor of 1.25 is considered by the Alberta Energy Regulator (AER) for calculating MOP for shallow thermal in situ oil sands applications (AER Bulletin, 2014). Considering the safety factor of 1.25, the predicted MOP for the isotropic and anisotropic models would be 2,045 and 1,913 kPa, respectively. These pressures are still higher than the operating pressure of 1,650 kPa exercised in the field.

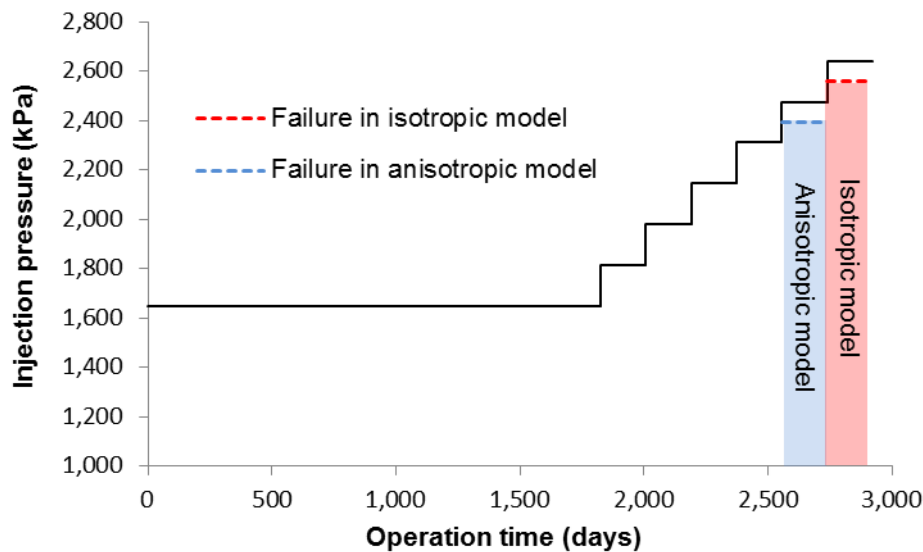


Figure 14. Sequences of injection pressure in both isotropic and anisotropic models

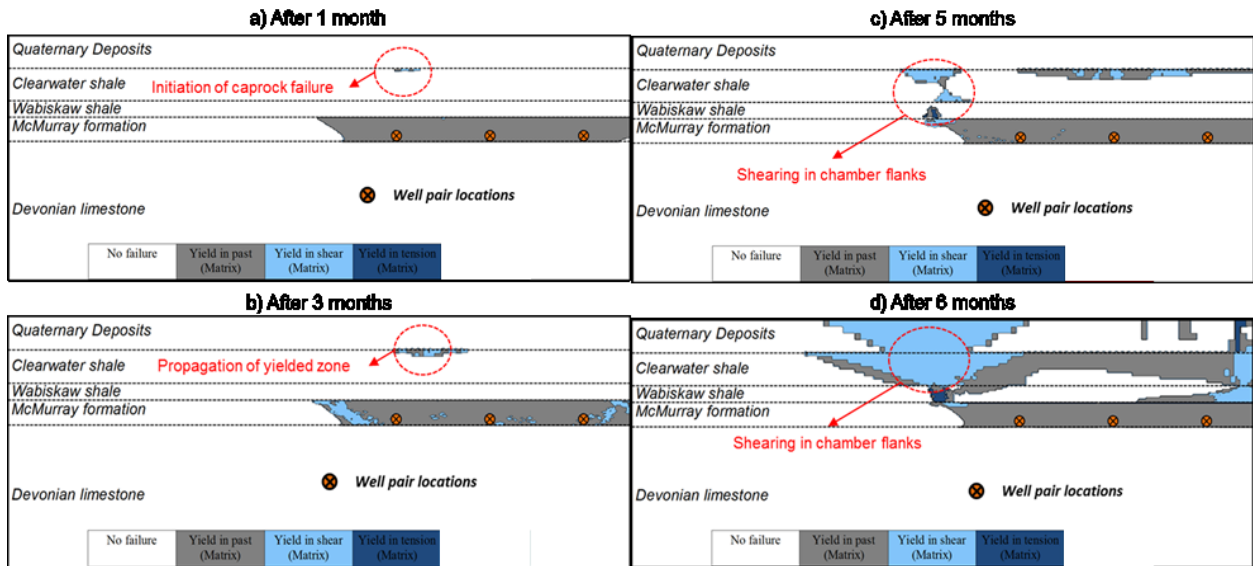


Figure 15. Yielded zones for anisotropic model at injection pressure of 2,392 kPa: a) after 1 month, b) after 3 months, c) after 5 months and d) after 6 months

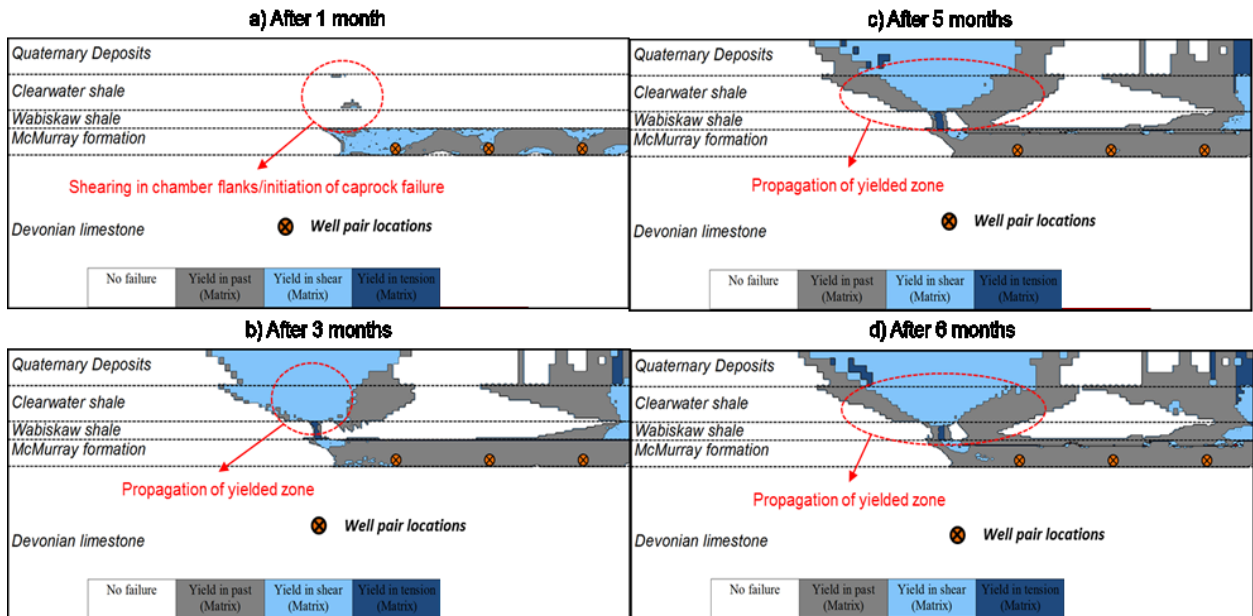


Figure 16. Yielded zones for isotropic model at injection pressure of 2,557 kPa: a) after 1 month, b) after 3 months, c) after 5 months and after d) after 6 months

5. Conclusion

A coupled hydro-thermo-mechanical model was introduced and employed in a case study to determine the failure pressure, hence the MOP, for a SAGD case study. Two cases were considered with isotropic and anisotropic cap shales to study the effect of neglecting shale intrinsic anisotropy on the MOP. Surface heave displacements were used to validate the model. The anisotropic model predicted closer surface heave displacement to the measurements.

Injection pressures during five years of operation did not result in the loss of caprock integrity for this case study for either of isotropic and anisotropic models. To determine the MOP, a scenario

was designed to sequentially increase the injection pressure beyond the MOP that had been exercised in the field. Each injection pressure was kept for six months. Results show higher MOP for the isotropic model. Results showed that the MOP for this case study was 45% and 55% higher than the peak operating injection pressure for anisotropic and isotropic models, respectively.

The results have shown that the anisotropic behavior of the caprock shales cannot be ignored in the simulations as common isotropic models provide an optimistic assessment of the MOP, approximately 7% higher than the anisotropic model.

Results also indicate caprock yield is time sensitive. In other words, yield may not start and propagate immediately after the injection pressure is increased to a certain level. After the pressure increase, it may take some time for the yield to start and some additional time for the yielded zone to grow in the entire thickness of the caprock. The results of the coupled model show that the initiation of caprock yield happens in the first three months of the ramp up of injection pressure and the caprock breach happens in the first six months of the ramp up keeping the same steam injection pressure.

Nomenclature

A, B, C, D	=	Constants in McLamore and Gray strength criterion
β	=	Constant in Touhidi-Baghini equation, MPa
c	=	Cohesion, kPa
C_{ijkl}	=	Compliance tensor
E_i	=	Young's modulus in i direction, MPa
ε_{ij}^e	=	Elastic strains tensor
G_{nv}	=	Cross-shear modulus, MPa
γ_P	=	Plastic shear strain
θ	=	Angle between plane of anisotropy and maximum principal stress
K	=	Permeability, mD
m, n	=	Anisotropy type factors
φ	=	Friction angle, °
σ'_1 and σ'_3	=	Maximum and minimum principal effective stresses, kPa
ν_{ab}	=	Poisson's ratio
ϕ	=	Porosity
σ_{lk}	=	Stress tensor, kPa
ε_V	=	Volumetric strain
ψ	=	Dilation angle, °

Acknowledgment

The authors would like to acknowledge the research funding for this study provided by NSERC through CRDPJ 387606-09.

References

AER, 2014. *Geological Characterization of the Lower Clearwater Shale in the Athabasca Oil Sands Area, Townships 87-99, Ranges 1-13, West of the Fourth Meridian*. Retrieved from http://www.ags.gov.ab.ca/publications/OFR/PDF/OFR_2014_04.PDF.

AER Bulletin, 2014. *Regulatory Approach for Shallow Thermal In Situ Oil Sands Applications in the Wabiskaw-McMurray Deposit of the Athabasca Oil Sands Area*. January, Retrieved from <https://www.aer.ca/documents/bulletins/AER-Bulletin-2014-03.pdf>.

Azad, A., and Chalaturnyk, R.J. 2011. Numerical Study of SAGD: Geomechanical-Flow Coupling for Athabasca Oil Sands Reservoirs. In 45th US Rock Mechanics/Geomechanics Symposium, San Francisco, California, 26-29 June. ARMA-11-414.

Bell, J.S., and Babcock, E.A. 1986. The Stress Regime of the Western Canadian Basin and Implications for Hydrocarbon Production. *Bulletin of Canadian Petroleum Geology*, **34**(1): 364-378.

Chalaturnyk, R.J. 2011. Observations on SAGD Caprock Integrity. In Recovery-2011 CSPG CSEG CWLS Convention.

Chalaturnyk, R.J. 1996. *Geomechanics of the Steam-Assisted Gravity Drainage Process in Heavy Oil Reservoirs*. PhD thesis, University of Alberta, Edmonton, Canada (April 1996).

CMG, 2013. *STARS 2013.11*, User Manual.

Collins, P.M. 2007. Geomechanical Effects on the SAGD Process. *SPE Reservoir Evaluation and Engineering*. **10**(4): 367-375. SPE-97905-PA.

Donath, F.A. 1964. *Strength Variation and Deformational Behavior in Anisotropic Rock*. State of the Earth in the Earth's Crust. New York: Elsevier, 281-98.

Duveau, G., Tiantang, Y., and Shao, J.F. 2001. Modelling of Anisotropy in Elastoplastic Sedimentary Rocks. In DC Rocks 2001 the 38th US Symposium on Rock Mechanics (USRMS), Washington D.C., 7-10 July. ARMA-01-1517.

ERCB, 2010. *ERCB Staff Review and Analysis: Total E&P Canada Ltd., Surface Steam Release of May 18, 2006, Joslyn Creek SAGD Thermal Operation*. Retrieved from https://www.aer.ca/documents/reports/ERCB_StaffReport_JoslynSteamRelease_2010-02.pdf

Hemsing, D.B. 2007. *Laboratory Determination of Seismic Anisotropy in Sedimentary Rock from the Western Canadian Sedimentary Basin*. MS thesis, University of Alberta, Edmonton, Canada (Fall 2007).

Hoek, E. 1964. Fracture of Anisotropic Rocks. *Journal of the South African Institute of Mining and Metallurgy*, **64**(10):510-518.

- Horino, F.G. and Ellickson, M.L. 1970. *A Method for Estimating Strength of Rock Containing Planes of Weakness*. Vol. 7449. US Dept. of Interior, Bureau of Mines.
- Itasca Consulting Group, 2011. *FLAC (Fast Lagrangian Analysis of Continua) User's Guide*. 5th. Vol. 7. Minneapolis, Minnesota: Itasca Consulting Group Inc.
- Karakul, H., Ulusay, R. and Isik, N.S. 2010. Empirical Models and Numerical Analysis for Assessing Strength Anisotropy Based on Block Punch Index and Uniaxial Compression Tests. *International Journal of Rock Mechanics and Mining Sciences*, **47**(4): 657-665.
- Khan, S., Han, H., Vishteh, M., and Khosravi, N. 2011. Caprock Integrity Analysis in Thermal Operations: An Integrated Geomechanics Approach. In WHOC-609 Proceedings for the 2011 World Heavy Oil Congress, Edmonton, Alberta. WHOC-11-609.
- Kosar, K.M. 1989. *Geotechnical Properties of Oil Sands and Related Strata*. PhD thesis, University of Alberta, Edmonton, Canada (January 1989).
- Kwasniewski, M.A. 1993. Mechanical Behavior of Transversely Isotropic Rocks. *Comprehensive Rock Engineering*, Vol. 1., pp. 285–312, New York: Oxford, Pergamon Press.
- Lekhnitskii, S.G. 1981. *Theory of Elasticity of an Anisotropic Body*, translated from the revised 1977 Russian edition, Mir, Moscow.
- Li, P., and Chalaturnyk, R.J. 2005. Geomechanical Model of Oil Sands. In PS-CIM/CHOA International Thermal Operations and Heavy Oil Symposium, Calgary, Alberta, 1–3 November. SPE-97949-MS. <http://dx.doi.org/10.2118/97949-MS>.
- McLamore, R., and Gray, K.E. 1967. The Mechanical Behavior of Transversely Isotropic Sedimentary Rocks. *Journal of Engineering for Industry*, **89**(1): 62–73.
- McLellan, P., and Gillen, K. 2000. Assessing Caprock Integrity for Steam-Assisted Gravity-Drainage Projects in Heavy-Oil Reservoirs. GEM Presentation, prepared for presentation at the (2000).
- Michiel H., 2001, *Spline interpolation*, Encyclopedia of Mathematics, Springer, ISBN 978-1-55608-010-4.
- Niandou, H., Shao, J.F., Henry, J.P., and Fourmaintraux, D. 1997. Laboratory Investigation of the Mechanical Behaviour of Tournemire Shale. *International Journal of Rock Mechanics and Mining Sciences*, **34**(1): 3-16.
- Nouri, A., Kuru, E., and Vaziri, H. 2009. Elastoplastic Modelling of Sand Production Using Fracture Energy Regularization Method. *Journal of Canadian Petroleum Technology*, **48**(04): 64-71.
- Petro-Canada Corp., 2005a. *Amendment Application for MacKay River Expansion: Project Description*. Retrieved from <http://citeseerx.ist.psu.edu/viewdoc/download?doi=10.1.1.116.729&rep=rep1&type=pdf>.
- Petro-Canada Corp., 2005b. *MacKay River Oilsands Progress Report*, Retrieved from <http://www.aer.ca/data-and-publications/activity-and-data/in-situ-performance-presentations>.
- Pettijohn, F. J. 1957, *Sedimentary rocks*, New York: Harper and Row, Third edition.

- Puzrin, A.M. 2012. *Constitutive Modelling in Geomechanics*. Zurich, Switzerland: Springer.
- Rahmati, E., Nouri, A., and Fattahpour, V. 2014. Caprock Integrity Analysis during a SAGD Operation Using an Anisotropic Elasto-Plastic Model. In SPE Heavy Oil Conference, Calgary, Alberta, 10-12 June. SPE-170114-MS.
- Rahmati, E., Nouri, A., and Rahmati, H. 2013. Numerical Assessment of Caprock Integrity in SAGD Operations. In SPE Heavy Oil Conference, Calgary, Alberta, 11-13 June. SPE-165422.
- Ramamurthy, T. 1993. Strength and Modulus Responses of Transversely Isotropic Rocks, *Comprehensive Rock Engineering*, Vol. 1, pp. 313-329 U.K.: Pergamon Press.
- Smith, R.J. 1997. *Geomechanical Effects of Cyclic Steam Stimulation on Casing Integrity*. MS thesis, University of Calgary, Calgary, Canada (Fall 1997).
- Sone, H. 2012. *Mechanical Properties of Shale Gas Reservoir Rocks and Its Relation to the In-situ Stress Variation Observed in Shale Gas Reservoirs*. PhD thesis, Stanford University, California, US (March 2012).
- Southern Pacific Resource Corp. 2012. *Annual Performance Presentation McKay River Thermal Project*. Retrieved from http://www.aer.ca/documents/oilsands/in_situ-presentations/2012AthabascaSouthernPacificMckaySAGD11461.pdf.
- Suncor Energy Inc. 2009. *MacKay River Performance Presentation*. Retrieved from http://www.aer.ca/documents/oilsands/in_situ-presentations/2009AthabascaSuncorMacKayRiver8668.pdf.
- Suncor Energy, 2013. *2013 AER Performance Presentation: Surface Commercial Scheme Approval No. 8668*. Retrieved from <http://www.aer.ca/documents/oilsands/insitu-presentations/2013SuncorMacKayRiver8668.pdf>.
- Thomas, S., and Sands, I.S.O. 2010. *Re: Project Update for Alberta Oilsands Inc. Clearwater West LP-SAGD Pilot Project*. Retrieved from http://www.aboilsands.ca/_pdfs/AOS-ERCB-Project-Update-Dec-13.pdf.
- Touhidi-Baghini A. 1998. *Absolute Permeability of McMurray Formation Oil Sands at Low Confining Stresses*. PhD thesis. University of Alberta, Edmonton, Canada (October 1998).
- Tutuncu, A.N. 2010. Anisotropy Compaction and Dispersion Characteristics of Reservoir and Seal Shales. In 44th US Rock Mechanics Symposium and 5th US-Canada Rock Mechanics Symposium, Salt Lake City, Utah, 27-30 June, ARMA-10-344.
- Uwiera-Gartner, M., Carlson, M.R., Walters, D.A., and Palmgren, C.T. 2011. Geomechanical Simulation of Caprock Performance for a Proposed Low Pressure Steam-Assisted Gravity Drainage Pilot Project. In Canadian Unconventional Resources Conference, Calgary, Alberta, 15-17 November. SPE-148886-MS.
- Walters, D.A., Wang, J., and Settari, A. 2012. A Geomechanical Methodology for Determining Maximum Operating Pressure in SAGD Reservoirs. In SPE Heavy Oil Conference Canada, Calgary, Alberta, 15-17 November. SPE-157855-MS.